Sheetlike structure in the proximity of compact DNA

Garima Mishra* and Somendra M. Bhattacharjee†
Department of Physics, Ashoka University, Sonepat 131029, India

(Received 31 May 2023; accepted 22 January 2024; published 16 February 2024)

We determine the phase diagram of DNA with inter- and intrastrand native-pair interactions that mimic the compaction of DNA. We show that DNA takes an overall sheetlike structure in the region where an incipient transition to a compact phase would have occurred. The stability of this phase is due to the extra entropy from the folding of the sheet, which is absent in the remaining polymerlike states of the phase diagram.

DOI: 10.1103/PhysRevE.109.024409

I. INTRODUCTION

A common bacterium such as a rod-shaped *E. coli* of size 2 μm × 1 μm × 1 μm stores a 1.5-mm-long DNA of $N = 4 \times 10^6$ base pairs. Even if the DNA takes an entropy-driven random coil form, its size $\sim\sqrt{N} \sim 5$ μm would still be too large to fit in the cell [1]. The evolutionary strategy of encapsulating protein-compactified chromosomes in a nucleus encased by membranes, as in eukaryotes, does not apply to prokaryotes that lack a nucleus, but still, compaction would resolve the DNA-packing puzzle. Over the years, with support from the dynamic light scattering [2] and the high-resolution single-molecule imaging [3] studies, the proposal of a boundaryless region called a nucleoid [4,5] is gaining ground, which creates an environment for DNA to collapse into a compact form.

DNA in a salt solution behaves as a polymer in a good solvent, called the swollen or coil phase, where excluded volume interactions dominate the overall behavior [6,7]. A surprising result was that a long DNA, much larger than its persistence length, can be collapsed into a compact shape [8] by adding ethanol, different types of cations, hydrophilic polymers, or organic solvents [9–11]. The collapse of DNA remained elusive in earlier studies because of the requirement of large lengths, though the tendency of liquid-crystalline ordering [12] was recorded for oligonucleotides. This tendency of local arrangement persists in the collapsed phase [8], suggesting the condensed DNA phase [13] to be different from the globular (collapsed) phase of a polymer below the theta point [6]. Moreover, as all base pairs should be easily accessible, an ordered or correlated structure would have a functional advantage. Consequently, a fractal globule phase has been proposed as a possible phase, where DNA is compact but without any knots [14]—a phase different from the usual compact globule. Such a fractal phase with power-law correlations of monomers finds support in the human genome [15].

As a tertiary structure of DNA, the compact phase is found to be insensitive to the secondary structure such as B, A, or Z [16]. DNA also undergoes a temperature- (or *p*H-) induced melting transition and a force-induced unzipping transition, both involving cooperative breaking of the hydrogen bonds of the base pairs [17]. In a bacterial environment, melting or unzipping is required for replication and, at least locally, for transcription to make the bases accessible. With the DNA in the nucleoid, a question arises: Does a compact DNA melt? Thus the phenomenon of DNA compaction in nucleoids is a topic of interest in biology, polymer physics, and also for practical applications because of the ease of insertion of a compact DNA in biosystems, e.g., in gene therapy [18].

The compaction phenomenon has been studied in some detail by treating DNA as polymers or polyelectrolytes. For example, a recent study focused on the melting temperature variations in the presence of attraction exclusively between bound pairs [19]. Other proposals include compaction induced by phase separation, mechanisms based on neutralizing charges on DNA, or the presence of small cations in solutions [4]. In Sec. II, we introduce the model and the details of the simulation. The various phases and the phase diagram are determined in Sec. III where a heuristic argument is also presented to motivate the phases. The summary and findings are in Sec. IV. Some of the details are given in the Supplemental Material [25] in the form of figures.

II. MODEL AND METHOD

We explore how compaction modifies double-stranded DNA (dsDNA) melting. The interactions are chosen to favor a folded conformation of dsDNA, thereby avoiding a generic globular phase in a poor solvent. Our coarse-grained model consists of two single-stranded DNA (ssDNA), A and B (also called polymers), with native DNA base pairing and an additional intrastrand base-pairing-type interaction that allows each polymer to fold on itself. The model potential considered for polymer A or B is

$$\left.\begin{matrix} E_{\rm A}/k_BT \\ E_{\rm B}/k_BT \end{matrix}\right\} = \sum_{i=1}^{N-1} K(d_{i,i+1} - d_0)^2 + 4\sum_{\text{N-nat}} \left(\frac{\sigma_{i,j}}{d_{i,j}}\right)^{12} + 4\epsilon_s \sum_{\text{N.C.}} \left[\left(\frac{\sigma_{i,j}}{d_{i,j}}\right)^{12} - \left(\frac{\sigma_{i,j}}{d_{i,j}}\right)^{6}\right], \quad (1)$$

where N.C. and N-nat denote native and non-native contacts. Here, each polymer consists of $N(= 36)$ beads, and the

*garima.mishra@ashoka.edu.in
†somendra.bhattacharjee@ashoka.edu.in

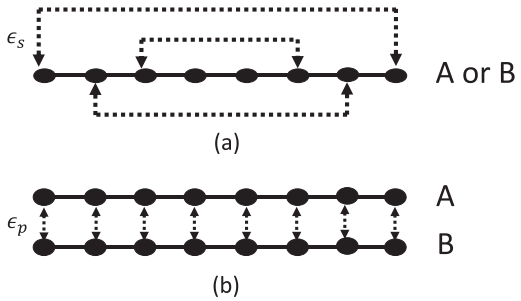

FIG. 1. Schematic diagram for the native contacts: (a) intrastrand contacts (dotted lines) in each polymer chain (A or B) with energy ϵ_s and (b) base-pair contacts (dotted lines) between chains A and B with energy ϵ_p.

distance between beads $d_{i,j}$ is defined as $|\boldsymbol{r}_i - \boldsymbol{r}_j|$, where $\boldsymbol{r}_i$ and $\boldsymbol{r}_j$ are the position vectors of beads i and j, respectively, with $i, j \in [1, N]$. We use dimensionless distances with $\sigma_{i,j} = 1$ and $d_0 = 1.12$. The energy parameters in the Hamiltonian are in units of k_BT where k_B is the Boltzmann constant and T is the temperature. The harmonic (first) term on the right-hand side (rhs) with a dimensionless spring constant $K(= 100)$ couples the adjacent beads along the chain [20,21]. The second term is a repulsive potential that prevents the overlap of non-native pairs of monomers of chain A (and B) [21–23]. The third term is the van der Waals energy (involving ϵ_s) that allows pairing of nonbonded monomers at position i and $N - i + 1$ [Fig. 1(a)]. These intrastrand pairings are the native contacts (N.C.) in Eq. (1). The interstrand interactions are given by

$$\frac{E_{\mathrm{A,B}}}{k_BT} = \sum_{\mathrm{N.C.}} 4\epsilon_p \left[\left(\frac{\sigma_{i,j}}{d_{i,j}} \right)^{12} - \left(\frac{\sigma_{i,j}}{d_{i,j}} \right)^{6} \right] + \sum_{\mathrm{N\text{-}nat}} 4 \left(\frac{\sigma_{i,j}}{d_{i,j}} \right)^{12}. \tag{2}$$

The base pairing between chains A and B is considered using the first term on the rhs of Eq. (2). The native base-pair contacts [same i of both the chains; see Fig. 1(b)] are such that it results in a ladder structure of dsDNA [20,21]. The second repulsive term of the potential energy in Eq. (2) prevents non-native pairings of monomers of chains A and B [20–23]. We obtain the dynamics of system by solving the set of Brownian equations [24]

$$\frac{d\boldsymbol{r_i}}{dt} = \frac{1}{\zeta}(\boldsymbol{F}_c + \boldsymbol{\Gamma}). \tag{3}$$

Here, $\boldsymbol{F}_c = -\boldsymbol{\nabla} E$ is the conservative force and E is the sum of E_{A}, E_{B}, and $E_{\mathrm{A,B}}$. ζ is the friction coefficient, set to 50, and $\boldsymbol{\Gamma}$ is the random force, a white noise with zero mean and correlation $\langle \Gamma_i(t)\Gamma_j(t')\rangle = 2\zeta k_BT\delta_{i,j}\delta(t - t')$. The temperature of the simulation is set to be constant $T = 0.16$. These equations of motion are integrated via the Euler method with time step $\delta t = 0.0015$. The initial structure for simulation is a ladderlike structure where chains are in proximity. To ensure equilibrium at different ϵ_s and ϵ_p, we performed 20 independent simulations, each spanning a total of 10^8 time steps.

III. RESULTS

A. Phase diagram in ϵ_s-ϵ_p plane

To understand the phase behavior, let us consider a simpler model with energy based on contact numbers. The interaction energy can be written as

$$\frac{E}{k_BT} = -\epsilon_p n_{\mathrm{AB}} - \epsilon_s(n_{\mathrm{AA}} + n_{\mathrm{BB}}), \tag{4}$$

where n_{AB} is the number of native base pairs between the two chains, with $-\epsilon_p$ as the energy for each pair, and $n_{\mathrm{AA}}, n_{\mathrm{BB}}$ are the number of intrastrand pairs with $-\epsilon_s$ as the energy per intrastrand pair. For a given DNA, ϵ_s, ϵ_p change with temperature with $\epsilon_s/\epsilon_p = \mathrm{const}$.

In the ϵ_s-ϵ_p plane, there are four fixed points (FPs) or limiting points which are representatives of the four phases one would expect naively, viz.,

(1) State I: a denatured phase of two free ssDNA chains (FP: $\epsilon_s = \epsilon_p = 0$);

(2) State II: bound A-B as dsDNA in a swollen phase (FP: $\epsilon_s = 0, \epsilon_p = \infty$);

(3) State III: two folded ssDNA in the denatured phase (FP: $\epsilon_s = \infty, \epsilon_p = 0$);

(4) State IV: dsDNA in the folded state (FP: $\epsilon_s = \epsilon_p = \infty$).

Assuming an all-or-none state, i.e., either all pairs are formed or all broken, the free energy of phase I is $F_{\mathrm{I}}/k_BT = -S_{\mathrm{I}}$, while for phase II, it is $F_{\mathrm{II}}/k_BT = -N\epsilon_p - S_{\mathrm{II}}$, where S_{I} and S_{II} are the total entropies of the chains in the respective phases. A first-order transition then takes place at $\epsilon_p = (S_{\mathrm{I}} - S_{\mathrm{II}})/N$, and the phase boundary is expected to be vertical in the ϵ_s-ϵ_p plane. By symmetry, the transition from I to III should also be at the same value of ϵ_s, and the boundary is horizontal, independent of ϵ_p. Similar vertical or horizontal boundaries are expected for the III $\leftrightarrow$ IV and the II $\leftrightarrow$ IV transitions. Deviations from linearity might occur near the intersection of the four transition lines because of the proximity of other phases. Can there be other intermediate phases in this two-parameter phase diagram?

To address the above question, we obtained the phase diagram in the ϵ_s-ϵ_p plane from our simulation by monitoring the peak position in energy fluctuation as a function of intrastrand energy (ϵ_s) at a fixed base-pairing energy (ϵ_p) and vice versa. The phase boundary is plotted in Fig. 2. We obtain a horizontal phase boundary close to $\epsilon_s = 0.75$ for $\epsilon_p < 1.00$, which starts bifurcating into two branches for $\epsilon_p > 1.00$ (wider peak in energy fluctuations; see Fig. S1 in the Supplemental Material [25]). Similarly, we observe a vertical phase boundary close to $\epsilon_p = 0.75$ for $\epsilon_s < 0.80$, which starts bifurcating into two branches for $\epsilon_s > 0.80$ (Fig. S2 [25]). Overall, the phase diagram is symmetric, except for the point at which the bifurcation starts appearing in the phase diagram ($\epsilon_p > 1.00$, and $\epsilon_s > 0.80$). In addition to the horizontal and vertical boundaries, as suggested by the energy construct, we obtain two additional regions (Y regions) in the phase diagram (Fig. 2). The average over two boundaries of each Y region further corroborates the horizontal or vertical nature of the boundaries in the phase diagram. We investigated the finite-size effect of chain length on the phase diagram by considering larger system with $N = 144$. Our findings indicate that the phase diagram remains consistent (Fig. S5 [25]).

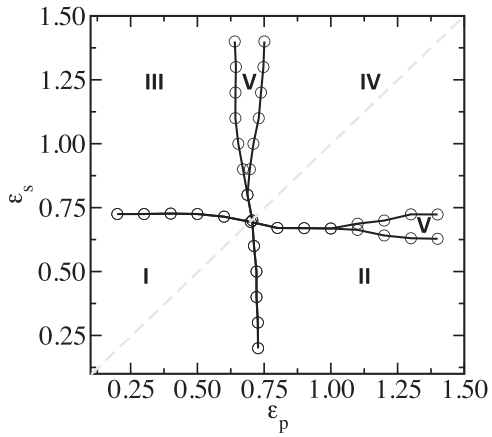

FIG. 2. The phase diagram shows the occurrence of various states in different regions of the ϵ_s-ϵ_p plane. These states are state I (two free ssDNA), state II (dsDNA), state III (two folded ssDNA), state IV (folded dsDNA), and state V (sheet). The dashed line corresponds to $\epsilon_s = \epsilon_p$ and goes through the intersection point of the phase boundaries.

B. Probability of occurrence of different phases

To get the microscopic view of the phase diagram, we probe the probability of occurrence of different structures in different regions of the phase diagram. The structures can be quantified by the number of base pairs (n_p) and the number of intrastrand pairs (n_s) present in a given conformation as below (the maximum number of allowed pairs is $n_{\max} = N$):

State I: n_p and n_s both are small ($<0.3n_{\max}$);
State II: large n_p ($>0.8n_{\max}$) and small n_s ($<0.3n_{\max}$);
State III: small n_p ($<0.3n_{\max}$) and large n_s ($>0.8n_{\max}$);
State IV: n_p and n_s both are large ($>0.8n_{\max}$).

The probability of occurrence of different states defined above ($P_{\rm I}$, $P_{\rm II}$, $P_{\rm III}$, and $P_{\rm IV}$) are plotted in Fig. 3. We see from Fig. 3(c) that $P_{\rm I} = 1$ for lower values of ϵ_p and ϵ_s and decreases as we increase ϵ_p or ϵ_s. For very large values of ϵ_p or ϵ_s, $P_{\rm I}$ becomes zero, and state II or state III starts appearing with small probabilities [Figs. 3(d) and 3(a)]. For larger values of ϵ_p and lower values of ϵ_s (the lower branch of the horizontal Y region), $P_{\rm II} = 1$ [Fig. 3(d)] while for larger values ϵ_s and lower values of ϵ_p (the left branch of the vertical Y region), $P_{\rm III} = 1$ [Fig. 3(a)], respectively. These states persist as we increase ϵ_p or ϵ_s. State IV starts appearing on the right of the vertical Y branch and above the horizontal Y branch, $P_{\rm IV} = 1$ [Fig. 3(b)] at larger values of ϵ_p and ϵ_s, with $P_{\rm IV} = 0$ elsewhere. Many mixed states (state VI) appear with finite probability ($P_{\rm VI}$) near the phase boundaries (coexistence line) (Figs. S3 and S4 [25]). The observations of states I–IV are in accordance with those predicted by the simple model of energy considered earlier. However, the simple model needs modifications to provide insight about the Y regions and the corresponding phases in the phase diagram.

It should be emphasized here that the vertical (horizontal) Y region starts appearing around intermediate values of $\epsilon_p(\epsilon_s)$, where a large energy $\epsilon_s(\epsilon_p)$ is already present in the system. A comparable energy scale may stabilize an intermediate phase between state III (state II) and state IV. As we cross the vertical Y region, n_s ($>0.8n_{\max}$) is almost unchanged (for large ϵ_s) and n_p goes from zero ($<0.3n_{\max}$ for small ϵ_p) to maximum ($>0.8n_{\max}$ for large ϵ_p). In the phase diagram, one may look further for a state with intermediate n_p and its occurrence probability. Motivated by this, we define a state V ($n_s > 0.8n_{\max}$ and $0.35n_{\max} < n_p < 0.6n_{\max}$). This state has a very high occurrence probability ($P_{\rm V} \sim 0.6$) as can be seen in the color map in Fig. 3(e), and it appears exactly in the vertical Y region of the phase diagram though it is absent elsewhere. This state V is a sheetlike structure [Fig. 3(e),

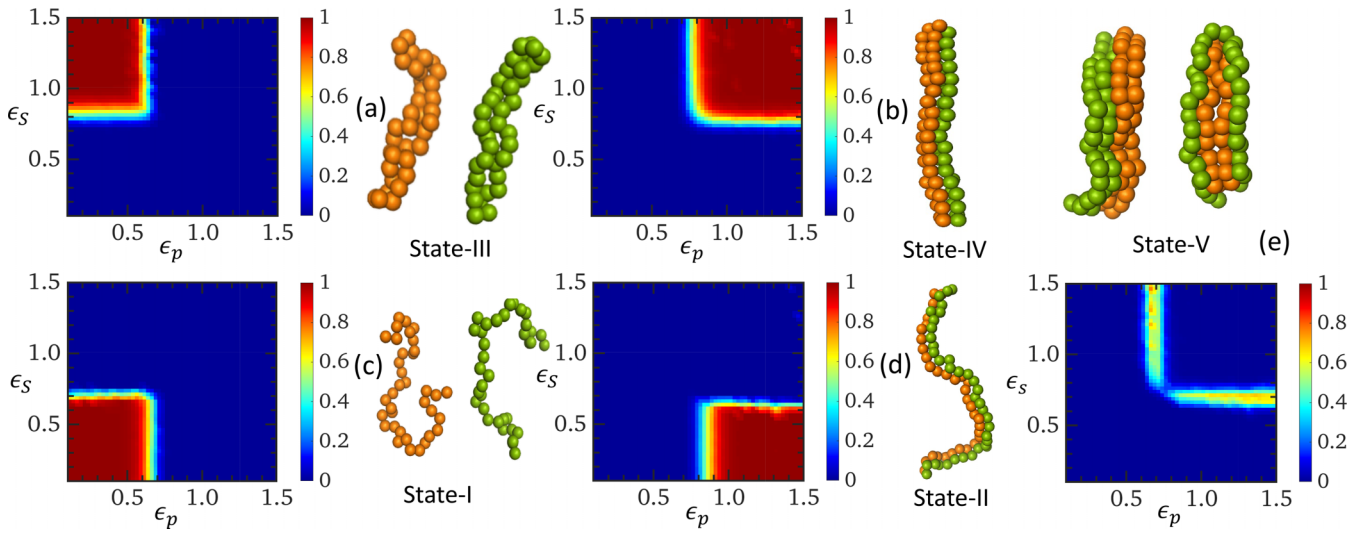

FIG. 3. The probability of occurrence of different states in the phase diagram. (a)–(d) The right panel shows four different states of polymer A (green) and polymer B (orange); state I (two free ssDNA), state II (one dsDNA), state III (two folded ssDNA), and state IV (folded dsDNA). In the left panel, the color map shows the probability of occurrence of a state (next to it) in different regions of the ϵ_s-ϵ_p plane. (e) A sheet structure formed from polymer A (green) and polymer B (orange) (top panel) and their occurrence probability in different regions of the ϵ_s-ϵ_p plane (bottom panel). The sheet structure occurs in the Y regions of the phase diagram.

upper left structure], formed as two folded ssDNA come close to each other. A similar sheetlike structure [$n_p > 0.8n_{\max}$ and $0.35n_{\max} < n_s < 0.6n_{\max}$, Fig. 3(e), upper right structure] occurs with high probability in the horizontal Y region, with the only difference that n_s and n_p flip their positions (large ϵ_p and comparable ϵ_s). In the presence of $\epsilon_p > 0.75$, the two polymer strands take on a flexible ladderlike configuration of DNA, state II. Notably, for very low native intrastrand pairing ($\epsilon_s < 0.60$), state II is more stable. As we increase ($\epsilon_s \geqslant 0.6$) one of the strands of DNA moves closer to the other by gaining enthalpy ϵ_s for each intrastrand pair. Importantly, this rearrangement occurs while maintaining the integrity of base pairing between two strands of DNA and results in the stabilization of the sheetlike structure (snapshots in Fig. S6 [25]). It is important to note here that two folded ssDNA (state III, for large ϵ_s) can be close to each other to form a sheet structure, without any geometrical constraint, by introducing bonds of comparable energy ϵ_p. However, forming the sheet from state II (large ϵ_p) is more difficult energetically. As the backbone of dsDNA (state II) consists of springs [first term of Eq. (1)], the formation of a sheetlike structure requires the stretching of a few springs at one side of the sheet. Therefore, the backbone always puts geometrical constraints on one side of the sheet. This extra geometric constraint results in the asymmetry in the starting points of vertical and horizontal Y regions.

The four states, states I–IV, are polymerlike. If s_0 is the entropy per monomer of a swollen polymer, we shall have, for the four states I–IV,

$$S_{\rm I} = 2Ns_0, \quad S_{\rm II} = Ns_0, \quad S_{\rm III} = 2\frac{N}{2}s_0, \quad \text{and} \quad S_{\rm IV} = \frac{N}{2}s_0.$$

The symmetry of the phase diagram follows from the phase boundaries

$$\epsilon_p|_{\rm I\to II} = s_0 \quad \text{and} \quad \epsilon_s|_{\rm I\to III} = s_0.$$

This picture is validated by more or less vertical or horizontal phase boundaries (Fig. 2), as explained above. In contrast to the four states, state V takes a flexible sheetlike structure with an extra source of entropy from the possibility of folding the sheet. The free energy of state V, with $S_{\rm V}$ as its entropy, is

$$\frac{F_{\rm V}}{k_BT} = -\frac{N}{2}\epsilon_p - N\epsilon_s - S_{\rm V}.$$

Therefore, the III-V and the IV-V transitions would take place at

$$\epsilon_p = 2(S_{\rm III} - S_{\rm V})/N \quad (\text{for III} \leftrightarrow \text{V}), \tag{5a}$$

$$\epsilon_p = 2(S_{\rm V} - S_{\rm IV})/N \quad (\text{for IV} \leftrightarrow \text{V}), \tag{5b}$$

which require $S_{\rm III} > S_{\rm V} > S_{\rm IV}$. In other words, state V would occur in the neighborhood of the putative III-IV transition. Similar arguments can be used for the II-IV phase boundary.

C. Melting of compact DNA

The replication and transcription process of DNA requires the separation of DNA strands. It is now well established experimentally and theoretically [17,24,26–31] that DNA undergoes a temperature- (or *p*H-) induced melting transition and a force-induced unzipping transition, both involving a cooperative breaking of the base pairs. To probe the melting transition of a compact DNA, we follow the evolution of different states by varying the interaction energy along the $\epsilon_p/\epsilon_s = 1$ line (the dashed line in Fig. 2). From our simulations, we compute the occurrence probabilities of different states (Fig. 4). We start with $\epsilon_s = \epsilon_p = 1.50$, where only state IV (folded dsDNA) appears with $P_{\rm IV} = 1$ until we are close to the intersection point in the phase diagram. Here, $P_{\rm IV}$ decreases, and many mixed configurations appear which we call state VI (see Fig. S4 [25]). As the intersection point is a coexistence point of at least four phases, many mixed configurations are expected to occur. In fact, we find $P_{\rm VI} \sim 1$ and $P_{\rm V} \sim 0.10$. The scenario changes as we go just below the intersection point of the phase diagram along the chosen line (Fig. 2). $P_{\rm I}$ starts picking up and state I becomes the only state ($P_{\rm I} = 1$) for lower values of ϵ_s. In short, we see the melting of a compact DNA along the chosen line. In contrast, for any other line with $\epsilon_p/\epsilon_s \neq 1$, the dsDNA to ssDNA transformation necessarily entails one other state.

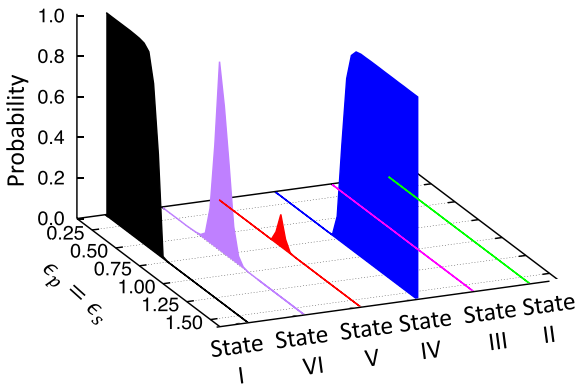

FIG. 4. Probability of occurrence of different states along the line with slope one ($\epsilon_s/\epsilon_p = 1$) in Fig. 2 (dashed line).

IV. CONCLUSIONS

In this paper, we studied the compaction of DNA by considering two types of effective interactions: (i) interstrand native-pair interactions that favor dsDNA formation, and (ii) intrastrand native-pair interactions that promote the folding of each strand of DNA. We studied a simpler case, employing a simplified native intrastrand interaction where a DNA segment can make only one native contact. The more intricate aspects of intrastrand interactions remain open for future investigations. The varying strengths of these effective interactions mimic the role of different cellular environments that lead to the compaction of DNA inside the cell.

We observed five different phases in the phase diagram as summarized in Fig. 2. There are transitions taking two free ssDNA (state I), at lower values of interaction energies, to either a bound dsDNA (state II) or two folded ssDNA (state III), as one of the interaction energies (intrastrand or interstrand) is increased, keeping the other one at a lower value. For larger values of both interaction energies, dsDNA folds onto itself (state IV), a state reminiscent of a compact DNA. If a heating process takes a compact DNA to ssDNA along a line through the intersection point, there will be a genuine melting point.

Otherwise another phase will always intervene. Furthermore, we observe from our simulations a sheetlike arrangement (state V); it occurs around the region where the III-IV or the II-IV transitions would have occurred and is unlike any of the other four states (I–IV), which are polymerlike. The stability of the phase comes from the extra folding entropy acquired by a sheetlike structure. It is important to note that the ladder model utilized in the present study lacks an inherent DNA twist, a fundamental characteristic of the DNA double helix. Nevertheless, a sheetlike phase in DNA is plausible if the entropy gain from transitioning from a twisted DNA to a sheetlike structure outweighs the enthalpic cost of untwisting of DNA. It would be interesting to probe the presence of sheetlike structures in future studies using a DNA model that incorporates DNA twist.

ACKNOWLEDGMENTS

G.M. gratefully acknowledges the financial support from Science and Engineering Research Board (SERB) India for a start-up grant with File No. SRG/2022/001771 and acknowledges the HPC computing facility at Ashoka University, Sonepat, India.

[1] The persistence length of DNA is $\xi = 50$ nm or 150 bp. The radius of gyration for a random walk of $N = 4 \times 10^6/150$ units each of length ξ is $R \sim \sqrt{N}\xi/\sqrt{6} \sim 5$ μm. One may take the Kuhn units of length 2ξ, but that does not affect the order of magnitude estimate. If the excluded volume interactions are taken into account, the size of the swollen conformation would be much larger. If excursions beyond the average size is taken into account, the actual size would be larger than the estimate above.

[2] R. S. Dias, J. Innerlohinger, O. Glatter, M. G. Miguel, and B. Lindman, J. Phys. Chem. B **109**, 10458 (2005).

[3] M. Stracy, S. Uphoff, F. Garza de Leon, and A. N. Kapanidis, FEBS Lett. **588**, 3585 (2014).

[4] M. Joyeux, J. Phys.: Condens. Matter **27**, 383001 (2015).

[5] S. C. Verma, Z. Qian, and S. L. Adhya, PLoS Genet. **15**, e1008456 (2019).

[6] S. M. Bhattacharjee, A. Giacometti, and A. Maritan, J. Phys.: Condens. Matter **25**, 503101 (2013).

[7] F. Valle, M. Favre, P. De Los Rios, A. Rosa, and G. Dietler, Phys. Rev. Lett. **95**, 158105 (2005).

[8] V. A. Bloomfield, Curr. Opin. Struct. Biol. **6**, 334 (1996).

[9] V. B. Teif and K. Bohinc, Prog. Biophys. Mol. Biol. **105**, 208 (2011).

[10] F. Ke, Y. K. Luu, M. Hadjiargyrou, and D. Liang, PLoS One **5**, e13308 (210).

[11] S. V. Mikhailenko, V. G. Sergeyev, A. A. Zinchenko, M. O. Gallyamov, I. V. Yaminsky, and K. Yoshikawa, Biomacromolecules **1**, 597 (2000).

[12] A. Leforestier and F. Livolant, Biophys. J. **65**, 56 (1993).

[13] The words "compact DNA" and "condensed DNA" will be used interchangeably. Similarly, DNA condensation and DNA compaction are used synonymously.

[14] A. Y. Grosberg, S. K. Nechaev, and E. I. Shakhnovich, J. Phys. France **49**, 2095 (1988).

[15] E. Lieberman-Aiden, N. L. van Berkum, L. Williams, M. Imakaev, T. Ragoczy, A. Telling, I. Amit, B. R. Lajoie, P. J. Sabo, M. O. Dorschner, R. Sandstrom, B. Bernstein, M. A. Bender, M. Groudine, A. Gnirke, J. Stamatoyannopoulos, L. A. Mirny, E. S. Lander, and J. Dekker, Science **326**, 289 (2009).

[16] S. Hormeño, F. Moreno-Herrero, B. Ibarra, J. L. Carrascosa, J. M. Valpuesta, and J. R. Arias-Gonzalez, Biophys. J. **100**, 2006 (2011).

[17] S. M. Bhattacharjee, J. Phys. A: Math. Gen. **33**, L423 (2000).

[18] H. G. Hansma, R. Golan, W. Hsieh, C. P. Lollo, P. Mullen-Ley, and D. Kwoh, Nucleic Acids Res. **26**, 2481 (1998).

[19] D. Majumdar, J. Stat. Phys. **190**, 14 (2023).

[20] G. Mishra, D. Giri, M. S. Li, and K. Sanjay, J. Chem. Phys. **135**, 035102 (2011).

[21] S. Kumar and G. Mishra, Phys. Rev. Lett. **110**, 258102 (2013).

[22] M. P. Allen and D. Tildesley, *Computer Simulations of Liquids* (Oxford Science, Oxford, UK, 1987).

[23] D. Frenkel and B. Smit, *Understanding Molecular Simulation* (Oxford Science, Oxford, UK, 1987).

[24] S. Kumar and M. S. Li, Phys. Rep. **486**, 1 (2010).

[25] See Supplemental Material at http://link.aps.org/supplemental/10.1103/PhysRevE.109.024409 for the following additional figures: (i) a graph depicting energy fluctuations as function of ϵ_s at various ϵ_p values, (ii) a graph depicting function of ϵ_p at various ϵ_s values, (iii) the probability of occurrence of state-VI (mixed states), (iv) illustrations of selected conformations within state-VI (mixed state), (v) the phase diagram in the ϵ_p-ϵ_s plane for 144 base pairs DNA, and (vi) representative snapshots for sheet formation ($\epsilon_p = 1.25$ and $\epsilon_s = 0.60$) at different MD time step.

[26] C. ter Burg, P. Rissone, M. Rico-Pasto, F. Ritort, and K. J. Wiese, Phys. Rev. Lett. **130**, 208401 (2023).

[27] C. Danilowicz, Y. Kafri, R. S. Conroy, V. W. Coljee, J. Weeks, and M. Prentiss, Phys. Rev. Lett. **93**, 078101 (2004).

[28] S. J. Koch, A. Shundrovsky, B. C. Jantzen, and M. D. Wang, Biophys. J. **83**, 1098 (2002).

[29] S. Rudnizky, H. Khamis, O. Malik, A. H. Squires, A. Meller, P. Melamed, and A. Kaplan, Nucleic Acids Res. **46**, 1513 (2018).

[30] R. Kapri, Phys. Rev. E **86**, 041906 (2012).

[31] A. R. Singh and R. Granek, J. Chem. Phys. **145**, 144101 (2016).